Locational Marginal Pricing in Electricity Markets: A Methodological Framework for Economic Efficiency

E. SALINAS-VILLACIS[1], C. QUINATOA-CAIZA[1,2], J. ACURIO-MASABANDA[1]
[1]Universidad Técnica de Cotopaxi
Av. Simón Rodríguez, Sector San Felipe, Latacunga
ECUADOR

[2]Universidad de Jaén
Campus Las Lagunillas s/n, 23071 Jaén,
SPAIN

Abstract: This paper presents a methodology to determine Locational Marginal Prices (LMPs) in electricity markets by integrating DC optimal power flow (DC-OPF) with loss factor modeling based on system distribution factors. The proposed framework combines detailed AC power flow simulations in DIgSILENT PowerFactory, used to calculate total system losses, with an optimization model implemented in Pyomo to capture the effects of transmission and generation constraints as well as marginal losses. Two DC-OPF models are formulated as follows: Model 1 without losses and Model 2 including loss factors derived from AC analysis. Results obtained for a simplified three-node system and the IEEE 39-node benchmark demonstrate that, under unconstrained conditions, LMPs converge to a uniform value, whereas transmission congestion introduces price differentials consistent with theoretical expectations. Incorporating marginal losses refines the pricing signals, ensuring a more accurate representation of real system operations. The proposed approach enhances computational efficiency while improving economic transparency, offering a robust tool for market operators and regulators to design and validate nodal pricing mechanisms.

Key-Words: Locational Marginal Prices, marginal cost, loss factor, distribution factor, optimization, spot pricing.

Received: January 6, 2026. Revised: March 2, 2026. Accepted: May 16, 2026. Published: July 21, 2026.

1 Introduction

The rise of renewable energy in power systems around the world aims to reduce CO_2 emissions. Electric power systems are undergoing digitalization and transformation through advanced digital technologies [1]. Consequently, the collection of system variables generates large datasets (big data) that can be exploited for predictive locational marginal price (LMP) forecasting using machine learning techniques [2]. However, when a method is well defined in terms of mathematical optimization, it often outperforms machine learning approaches. On the other hand, electricity market agents (EMAs) determine LMPs using the DC optimization model, which does not take system losses into account [3], or by applying AC optimization [4]. In the case of AC optimization, the balance equations are nonlinear and do not guarantee a global optimum. Nevertheless, in recent years convex optimization techniques have been applied to determine LMPs [5], [6].

In addition to the growing interest in optimization-based LMP computation, recent literature has emphasized that the quality of nodal prices depends not only on the mathematical formulation but also on how accurately physical grid constraints are represented. Several authors highlight that the interaction between renewable uncertainty, network topology, and operational flexibility amplifies the variability of LMPs, making traditional DC-based analyses less reliable in increasingly dynamic grids [7], [8]. Furthermore, studies in modern power systems point out that the increasing deployment of distributed generation and active distribution networks requires more detailed LMP formulations that capture downstream congestion, voltage limitations, and stochastic injections [9].

The other problems are network congestion and generation operating limits, which increase LMPs and the total cost of the power system [10],[11]. When transmission lines reach their thermal or stability limits, power flows must be redistributed, leading to nodal price separation and higher system costs [12]. Similarly, when generators hit their operational limits such as maximum or minimum capacity, ramping constraints, or reserve requirements the economic dispatch is forced to rely on more expensive units, raising overall LMPs [13]. These active constraints imply that LMPs reflect not only the marginal cost of energy but also the marginal cost of maintaining system reliability and physical feasibility.

To address the aforementioned problems related to LMPs, the scientific literature provides several relevant papers. In [14], the author develops a DC model without losses and a linearized AC model, and analyzes two systems (transmission and distribution) integrated with distributed generation. In [15], [16], the authors extend this approach with a focus on uncertainty. With respect to convex optimization, [17], [18], [19], [20], [21] compute LMPs using second-order cone programming with an approach based on Nash mechanisms. In [22] the author proposes replacing the traditional LMP approach with multi-interval nodal pricing mechanisms, which allow a more accurate representation of network flexibility and volumetric risk, thereby viewing the grid as an insurance mechanism that supports flexibility [23]. Although the LMP framework incorporates both congestion and losses in its calculations, the paper argues that its underlying logic remains static and incomplete [24], [25]. It does not adequately capture the real dynamics of energy delivery nor the associated systemic risks.

Despite this extensive body of work, recent reviews in electricity market design argue that current LMP methodologies still lack a unified treatment of marginal losses, uncertainty modeling, and multi-level coordination between transmission and distribution systems [26]. Moreover, several comparative studies indicate that while convex relaxations improve convergence and tractability, they may still misrepresent reactive power effects and voltage-dependent losses unless integrated with AC-based datasets [27]. These findings reinforce the need for hybrid methodologies that combine AC-accurate physical modeling with the computational efficiency of DC-based formulations.

Based on the previously reviewed problems and the state of the art, this study contributes to the advancement of LMPs methodologies by integrating AC-based [28] loss factor modeling with DC optimal power flow (DC-OPF) formulations [29]. Unlike conventional LMPs approaches that neglect marginal losses or simplify congestion modeling, this work bridges AC simulation precision with DC computational tractability using DIgSILENT PowerFactory [30] and Pyomo Optimization [31]. By validating both a simplified 3-node and a benchmark 39-node system, the framework demonstrates how transmission constraints and marginal losses jointly influence nodal prices.

Additionally, this paper expands the existing literature by providing a broader discussion on how loss factor modeling affects LMP transparency, risk allocation, and regulatory decision-making. The proposed methodology aligns with recent academic recommendations suggesting that future electricity markets require pricing mechanisms capable of integrating AC-accurate losses while maintaining scalability and computational consistency [32].

The study extends current literature by offering a reproducible, economically transparent methodology that enhances price accuracy under realistic grid conditions [33]. In addition, the proposed framework can be adapted to different regulatory contexts and market structures, making it a flexible tool for both developed and emerging electricity markets. Its modular design allows researchers to test alternative loss allocation schemes, assess the economic impact of network upgrades, and analyze future scenarios with high renewable penetration. Furthermore, the methodology provides a replicable bridge between commercial power system software and open-source optimization environments, enabling a wider community of academics, regulators, and industry practitioners to evaluate nodal pricing under realistic operating conditions.

The sections of the paper are organized as follows: The methodology is presented in Section II. The optimization model validation is described in Section III. The discussion of the results is given in Section IV. The scientific contribution is highlighted in Section V, and finally, the conclusion is provided in Section VI.

2 Problem Formulation

The proposed electric system is modeled in DIgSILENT, including the detailed representation of all elements in order to perform power flow analysis and thereby obtain a system state similar to the actual electrical network. Subsequently, data on loads, lines, transformers, generators, and other elements are extracted. These data are then prepared for the Pyomo optimizer, which is used to obtain the nodal price results, as shown in Figure 1.

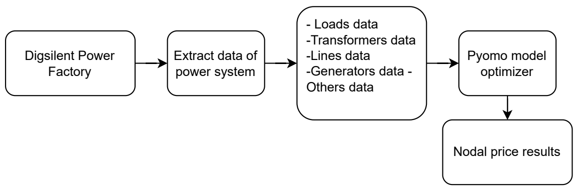

Figure 1: Steps to Determine LMPs
Source: created by the authors

In the literature, the mathematical models to obtain nodal prices in power systems take two forms:

- DC model optimization
- AC model optimization

The AC optimization model includes the nodal balance equations for active and reactive power. These equations are difficult to solve because they are nonlinear, and thus the optimal point is only local and uniqueness cannot be guaranteed. By contrast, the DC optimization model is an approximation of the AC model that can be solved much faster and generally finds a global optimum. Therefore, the equation presented corresponds to the DC optimization model.

Let $\mathcal{N}$ be the set of buses and $\mathcal{L}$ the set of transmission lines. For each line $m \in \mathcal{L}$, the ordered pair (i, j) defines its sending and receiving buses. Active power injections p_{gi} and demands d_i are specified at bus $i \in \mathcal{N}$. Voltage phase angles are denoted by θ_i for each $i \in \mathcal{N}$. Each transmission line is modeled with a single oriented flow variable f_m.

DC Model 1 We define the DC model no loss of the following way [34]:

$$\min z = \sum_{i \in \mathcal{N}} c_i * pg_i \quad (1)$$

subject to:

$$\sum_{i,j \in \mathcal{L}} f_{i,j} - \sum_{j,i \in \mathcal{L}} f_{j,i} + pg_i = d_i \ \ \forall i \in \mathcal{N} \quad (2)$$

$$f_{i,j} = v_i v_j (\theta_i - \theta_j)/x_{i,j} \ \ \forall i, j \in \mathcal{L} \quad (3)$$

$$|f_{i,j}| \leq f_{i,j}^{max} \ \ \forall i, j \in \mathcal{L} \quad (4)$$

$$pg_i^{min} \leq pg_i \leq pg_i^{max} \ \ \forall i \in \mathcal{N} \quad (5)$$

$$\theta_i^{min} \leq \theta_i \leq \theta_i^{max} \ \ \forall i \in \mathcal{N} \quad (6)$$

Equation (1) formulates the objective function aimed at minimizing the total generation cost. Equation (2) enforces the nodal power balance; in this expression, $f_{j,i}$ denotes the power flow entering node i from node j, which is simply the opposite orientation of $f_{i,j}$, this distinction is required to properly account for incoming and outgoing flows in the nodal power balance. Equation (3) characterizes the power flow through the transmission lines. Equation (4) imposes the upper limit on line power flows, Equation (5) specifies the maximum generation capacity of each unit, and Equation (6) restricts the voltage angle within its allowable range.

DC Model 2 We define the DC model with losses as follows:

$$\min z = \sum_{i \in \mathcal{N}} c_i * pg_i \quad (7)$$

subject to:

$$\sum_{i \in \mathcal{N}} LFg_i * pg_i - \sum_{i \in \mathcal{N}} LFd_i * d_i = PL + OFFSET \quad (8)$$

$$\sum_{i,j \in \mathcal{L}} f_{i,j} - \sum_{j,i \in \mathcal{L}} f_{j,i} + pg_i = d_i + PL \ \ \forall i \in \mathcal{N} \quad (9)$$

$$f_{i,j} = v_i v_j (\theta_i - \theta_j)/x_{i,j} \ \ \forall i, j \in \mathcal{L} \quad (10)$$

$$|f_{i,j}| \leq f_{i,j}^{max} \ \ \forall i, j \in \mathcal{L} \quad (11)$$

$$pg_i^{min} \leq pg_i \leq pg_i^{max} \ \ \forall i \in \mathcal{N} \quad (12)$$

$$\theta_i^{min} \leq \theta_i \leq \theta_i^{max} \ \ \forall i \in \mathcal{N} \quad (13)$$

Equation (8) represents the global system balance, where total generation and demand are adjusted by the loss factors (LF) so that their net difference equals the system losses (PL) plus an offset term. In this formulation, PL is a variable representing total transmission losses, ensuring that the overall power balance properly accounts for network losses and calibration adjustments. The OFFSET term is a corrective parameter introduced to guarantee the exact closure of the power balance equation in the DC model with losses. Because the loss factors (LF) result from linearizations or approximations, the computed sum of generation, demand, and estimated losses may not perfectly coincide. These small discrepancies lead to a residual mismatch in the system-wide balance equation. The OFFSET absorbs this residual error, allowing the model to maintain strict equality in the global balance constraint. As a result, the numerical consistency of the dispatch solution is preserved without altering the physical interpretation of the system or affecting the operational results. Equation (9), in turn, enforces the nodal power balance by requiring that, at each node, the sum of incoming and outgoing line flows plus local generation equals the local demand. The term PL appears only in the slack-node power balance equation, as the slack node is responsible for absorbing the total system losses.

In the proposed formulation, one bus is selected as the reference (slack) node to fix the voltage angle and absorb the residual mismatch associated with loss linearization. While the slack bus is responsible for balancing total system losses in the nodal equations, its selection does not alter the economic efficiency of the dispatch. In large-scale systems, however, the choice of slack affects the numerical values of distribution factors and loss factors, which in turn modifies the decomposition of LMPs into energy, congestion, and loss components. Importantly, although the absolute nodal prices may shift slightly due to loss allocation through the slack, price differentials between nodes which drive economic signals remain consistent. Therefore, the slack bus should be interpreted as a mathematical reference for loss allocation rather than an economically privileged location.

The generation loss factor (LFg) and the demand loss factor (LFd) represent the derivatives of the system losses with respect to power injections, which can be demonstrated as follows:

If we take Equation (9) and apply the Lagrangian method, deriving with respect to power injections. Where $f_{i,j} = f_{j,i} = f_m$:

$$\pi_i = \lambda + \lambda \frac{dL_m}{dpg_i} + \sum_{m \in \mathcal{L}} u_m \frac{df_m}{dpg_i} \tag{14}$$

This equation defines the nodal price, which consists of three components: the market price (λ), the loss price, and the congestion price. The derivative $\frac{dL_m}{dpg_i} = LFg$ is called the generation loss factor, while $\frac{dL_m}{dd_i} = LFd$ is the demand loss factor. The Lagrange multiplier u_m is used for line congestion, and $\frac{df_m}{dpg_i}$ represents the system's distribution factor.

To determine the loss factor, the following approximation is used:

$$Lm = R_m f_m^2 \tag{15}$$

where L_m denotes the loss in line m of the system, R_m is the resistance, and f_m is the power flow. If we take Equation (15) and compute its derivative with respect to the power injection, we obtain:

$$\frac{dL_m}{dpg_i} = 2\left(\sum_{m \in \mathcal{L}} R_m f_m H_{i,m}\right) \tag{16}$$

where $H_{i,m} = \frac{df_m}{dpg_i}$ is factor distribution. Therefore, the $H_{i,m}$ we obtain:

$$H_{i,m} = Y * A * (A^T * Y * A)^{-1} \tag{17}$$

where Y is the transfer susceptance matrix between nodes i and j , the A is incidence matrix line - node.

Numerical stability considerations. The matrix $H = A^\top Y A$ corresponds to a weighted Laplacian of the network and is therefore singular with rank $n-1$, reflecting the invariance of voltage angles to a uniform phase shift. To obtain a unique solution, one reference (slack) bus angle is fixed (typically $\theta_{\text{slack}} = 0$). This is implemented by removing the column of the incidence matrix A associated with the slack bus, yielding a reduced matrix $\tilde{A}$. The resulting matrix $\tilde{H} = \tilde{A}^\top Y \tilde{A}$ is full-rank and invertible. In large-scale networks, however, near-singularity may still arise due to weakly connected areas or very small line susceptances, leading to ill-conditioning of the linear system. In such cases, direct matrix inversion becomes numerically unstable and sparse factorization or regularization techniques are preferable.

2.1 Optimality preservation of the DC–OPF with linearized loss factors

The AC nodal active power balance can be expressed as

$$P_i^{AC}(\theta, V) = P_i^{DC}(\theta) + P_i^{loss}(\theta, V), \tag{18}$$

where P_i^{DC} is the lossless DC power flow approximation and P_i^{loss} represents the real power losses.

A first–order Taylor expansion around an operating point (θ^*, V^*) yields

$$P_i^{AC} \approx P_i^{DC} + \sum_{j \in \mathcal{N}} \frac{\partial P_i^{loss}}{\partial P_j} \Delta P_j + \text{OFFSET}. \tag{19}$$

Defining the loss factor

$$LF_{ij} = \frac{\partial P_i^{loss}}{\partial P_j}, \tag{20}$$

the power balance becomes

$$P_i^{AC} \approx P_i^{DC} + \sum_{j \in \mathcal{N}} LF_{ij} P_j + \text{OFFSET}. \tag{21}$$

Therefore, embedding loss factors into the DC–OPF corresponds to a first–order linearization of the AC power balance equations. The Karush–Kuhn–Tucker (KKT) conditions of the AC–OPF are

$$\nabla C(P_g^*) = \lambda^{AC} \nabla P^{AC}(P_g^*). \tag{22}$$

Since

$$\nabla P^{AC} = I + LF, \tag{23}$$

the proposed formulation imposes the same Jacobian matrix up to second–order terms, implying

$$\lambda^{DC+loss} = \lambda^{AC} + \mathcal{O}(\Delta^2). \tag{24}$$

Hence, the optimal dispatch obtained from the proposed DC–OPF with linearized losses preserves the economic optimality of the AC–OPF to first order.

2.2 Economic consistency of the LMP decomposition

The locational marginal price (LMP) is defined as the marginal cost of supplying an incremental demand at bus i,

$$\lambda_i = \frac{\partial C^*}{\partial d_i}. \tag{25}$$

When losses are considered, the global power balance is

$$\sum_{i \in \mathcal{N}} P_{gi} = \sum_{i \in \mathcal{N}} d_i + P^{loss}. \tag{26}$$

Taking the derivative of the optimal cost with respect to demand gives

$$\lambda_i = \lambda_0 \left(1 + \frac{\partial P^{loss}}{\partial P_i}\right) + \sum_{k \in \mathcal{L}} \mu_k PTDF_{k,i}, \quad (27)$$

where λ_0 is the system marginal energy price and μ_k are the shadow prices of transmission constraints.

Defining the loss factor

$$LF_i = \frac{\partial P^{loss}}{\partial P_i}, \quad (28)$$

the LMP can be written as

$$\boxed{\lambda_i = \underbrace{\lambda_0}_{\text{energy}} + \underbrace{\sum_{k \in \mathcal{L}} \mu_k PTDF_{k,i}}_{\text{congestion}} + \underbrace{\lambda_0 LF_i}_{\text{loss}}} \quad (29)$$

Thus, the proposed LMP decomposition corresponds to the first–order expansion of the AC marginal price and remains economically consistent, since the loss component represents the incremental generation required to compensate additional system losses caused by a marginal injection at bus i.

All the aforementioned equations are implemented in Python using Pyomo, following the procedure illustrated in Figure 2:

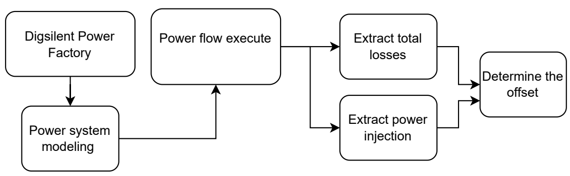

Figure 2: Nodal price with loss
Source: created by the authors

The procedure in DIgSILENT PowerFactory begins with the modeling of the power system, where all nodes, lines, and equipment are represented according to their electrical parameters. Once the model is established, the next step is to execute a power flow analysis to obtain voltages, currents, and system behavior under given operating conditions. From these results, the total system losses are extracted, providing an indication of efficiency. Subsequently, power injections at different nodes are identified, and the offset between calculated and expected values is determined, allowing the validation of the model and a precise assessment of system performance.

3 Optimization model validation

3.1 Tree node system

The validation system shown in Figure 3 consists of three 110 kV nodes connected by three transmission lines, each with a reactance of 0.25 p.u. and a resistance of 0.05 p.u., with Sbase of 100 MVA. The thermal capacity of each line is 1 kA. The system includes two generators: G1 with a maximum power of 500 MW and G2 with a maximum power of 300 MW with cost of 10 \$/h and 12 \$/h respectively. The total demand connected to the system is 150 MW.

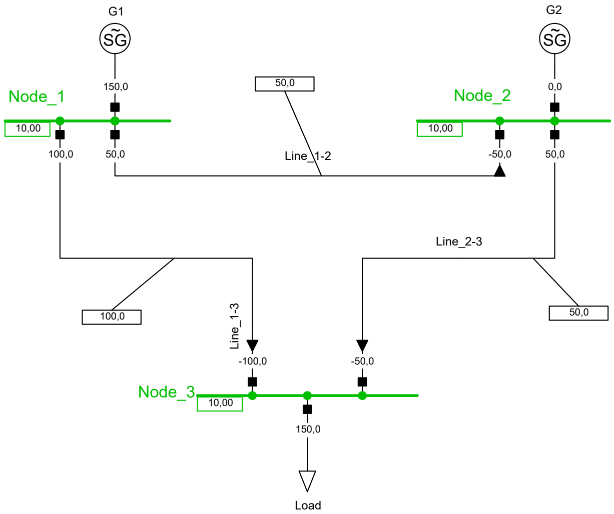

Figure 3: Nodal price without loss
Source: created by the authors

Using DC Model 1, which determines nodal prices without accounting for losses, the obtained results are presented in Table 1:

Table 1. DC Model 1 nodal prices.

Node	Price ($\$/MWh$)	P (MW)
N1	10	150
N2	10	0
N3	10	150

Source: created by the authors

The nodal prices are identical because the transmission lines have sufficiently large capacity. In this case, the Lagrange multiplier μ is not active, and the system losses are assumed to be zero.

To demonstrate congestion, the transmission line between nodes 1 and 2 is limited to 30 MW, while the remaining lines are set to 200 MW, similar to the previous case in Table 2 present the result.

Table 2. DC Model 1 nodal prices with constraints.

Node	**Price** (\$/MWh)	**P (MW)**
N1	10	120
N2	12	30
N3	11	150

Source: created by the authors

From the power flow simulation in Figure 4, it can be observed that the active power on line 1–3 is 90 MW, while on line 2–3 it is 60 MW. The nodal prices are different because the Lagrange multiplier is active only for line 1–2. Therefore, the price at each node reflects the marginal cost of generation; however, the price at node 3 is determined by the combined contribution of generators G1 and G2.

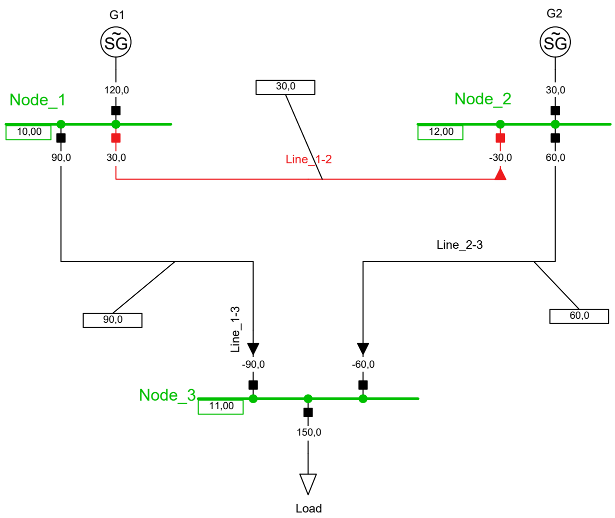

Figure 4: Nodal price without loss
Source: created by the authors

Using the DC Model 2, which incorporates transmission losses for nodal price determination, the obtained results are summarized as follows. First, an AC power flow was performed using the Newton–Raphson method in DIgSILENT PowerFactory, and the results are presented in Figure 5.

The power injections at Node 1 and Node 2 are 116.9 MW and 40 MW, respectively, while the total system loss is 6.9 MW. Nevertheless, in order to determine the offset, it is necessary to compute the loss factors, which are obtained from (16) and (17).

$$\mathbf{A} = \begin{bmatrix} L_{12} \\ L_{13} \\ L_{23} \end{bmatrix} \begin{bmatrix} 1 & -1 & 0 \\ 1 & 0 & -1 \\ 0 & 1 & -1 \end{bmatrix} \tag{30}$$

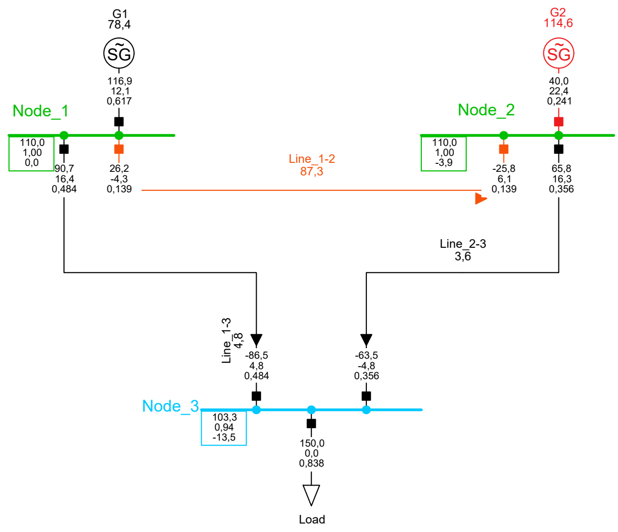

Figure 5: Nodal price without loss
Source: created by the authors

The equation 30 incidence matrix (line–node) is defined such that the element is equal to 1 when the power flow leaves the node, –1 when the power flow enters the node, and 0 otherwise. To construct the susceptance matrix Y equation (31), each element represents the susceptance between node i and node j.

$$\mathbf{Y} = \begin{bmatrix} y_{12} & 0 & 0 \\ 0 & y_{13} & 0 \\ 0 & 0 & y_{23} \end{bmatrix} \tag{31}$$

Finally, we obtain the distribution factor equation (32), taking node 1 as the slack node.

$$\mathbf{H} = \begin{bmatrix} 0 & -2/3 & -1/3 \\ 0 & -1/3 & -2/3 \\ 0 & 1/3 & -1/3 \end{bmatrix} \tag{32}$$

Applying Equation (16), we obtain the loss factors:

$$\mathbf{LF} = \begin{bmatrix} 0 \\ -0.030 \\ -0.09 \end{bmatrix} \tag{33}$$

OFFSET calculation. Using the base-case transmission losses of $P_{\text{loss}} = 6.9$ MW and the loss factors $(\text{LF}_1, \text{LF}_2, \text{LF}_3) = (0, -0.03, -0.09)$ applied to the corresponding nodal injections $(P_1, P_2, D_3) = (116.9, 40, -150)$ MW, the contribution of each node to the linearized loss estimation can be evaluated. Since node 1 is defined as the slack bus, it absorbs any mismatch between the linearized loss approximation and the actual system losses. By combining the base-case losses with the loss–factor-weighted injections, the resulting *OFFSET* term captures this residual imbalance and ensures that the global power-balance equation closes exactly. The computed OFFSET term is:

$$\begin{aligned}\text{OFFSET} &= 6.9\,\text{MW} - (0)(116.9\,\text{MW}) \\ -(-0.030)(40\,\text{MW}) &\quad - (-0.09)(-150\,\text{MW}) \\ &= 5.4\,\text{MW}.\end{aligned} \tag{34}$$

The computed OFFSET of 5.4 MW represents the net adjustment required to balance the system equations after accounting for measurement errors and modeling approximations. This value arises from the weighted contributions of nodal injections and withdrawals, reflecting both positive and negative deviations. A nonzero OFFSET indicates residual inconsistencies between observed data and estimated states, highlighting the importance of correction terms to preserve overall system feasibility.

The nodal prices derived from DC Model 2 are computed using equation (14) are present in Table 3:

Table 3. Nodal price including losses and congestion.

Node	Price ($\$/MWh$)	P (MW)
N1	10.00	127.2
N2	12.01	30.0
N3	11.755	-150.0

Source: created by the authors

Table 3 summarizes nodal results for a three-node distribution system. Node N1 exhibits a price of 10 \$/MWh with a positive injection of 127.2 MW, while Node N2 presents a slightly higher price of 12.01 \$/MWh and a moderate load of 30 MW. Conversely, Node N3 shows 11.755 \$/MWh with a withdrawal of 150 MW, illustrating price variations under different supply–demand conditions.

3.2 Error metrics

These metrics were compared with the loss factor values, since these factors are linearized or approximated. First, the loss factors were computed in DIgSILENT, and then obtained again using the approach proposed in this paper. They were not compared with nodal prices because the values are identical and differ only due to numerical rounding. The obtained values for MSE, RMSE, and MAE demonstrate a high level of consistency between both methods. The errors are on the order of 10^{-3}, indicating that the discrepancies are marginal and do not significantly affect the magnitude of the nodal results. Consequently, both methods can be considered equivalent for operational analysis, validation, or benchmarking purposes. In addition, these results reinforce the robustness of the proposed methodology, confirming that its simplified representation accurately captures the essential behavior of the system while maintaining computational efficiency—an important requirement for practical applications, large-scale studies, and real-time decision-making environments. The values are present in Table 4.

Table 4. Error metrics for the three-node comparison.

Load	MAE	RMSE	Relative Error (%)	MAPE (%)
60%	0.00075	0.00115	3.1	2.6
80%	0.00137	0.00191	3.6	3.1
100%	0.00367	0.00581	7.2	6.3
120%	0.00810	0.01299	12.9	11.0
140%	0.02727	0.04225	26.8	24.5

Source: created by the authors

Table 4 summarizes the accuracy of the evaluated approach under different loading conditions. For loading levels up to 80%, the errors remain very small (MAE < 0.0015 p.u., RMSE < 0.002 p.u., and Relative Error and MAPE below 4%), indicating an excellent approximation of the reference solution. At nominal loading (100%), the error slightly increases but still stays within acceptable limits for power system analysis (MAPE = 6.3%, Relative Error = 7.2%), confirming that the method preserves good fidelity around normal operating conditions. However, as the system becomes heavily loaded (120% and 140%), the error increases considerably, reaching MAE = 0.02727 p.u., RMSE = 0.04225 p.u., and percentage errors above 20% at 140% loading. This behavior is expected because the linearization assumptions progressively lose validity in stressed operating regimes where nonlinear power flow effects dominate. Overall, the results demonstrate that the method is reliable and accurate for light and nominal operating conditions, which correspond to typical system operation, while its performance deteriorates under heavily loaded scenarios.

3.3 IEEE 39-node

The IEEE 39-nodes New England test system [35] is a standard benchmark widely adopted for power market and operational studies. It consists of 39 nodes, 10 generating units, and 46 transmission lines, operating at a nominal voltage of 345 kV. The system supplies a total demand of approximately 6,300 MW, with generation resources distributed across multiple nodes and interconnected through a meshed transmission network. In addition to its realistic representation of transmission congestion and generation dispatch, this system provides a suitable platform for validating optimization algorithms, testing locational marginal pricing methodologies, and analyzing system reliability under diverse operational scenarios, making it an indispensable reference in electricity market research.

Node 31 is modeled as the reference (slack), while the remaining nodes are designated as load or generator nodes. The system's topology and operating conditions provide a realistic framework to evaluate congestion patterns, transmission constraints, and LMPs. Owing to its representative scale and complexity, the IEEE 39-node system is widely employed for validating nodal pricing methodologies and electricity market simulations. In the Fgure 6 reports the nodal prices obtained under the DC Model 1 formulation without considering losses or transmission line constraints.

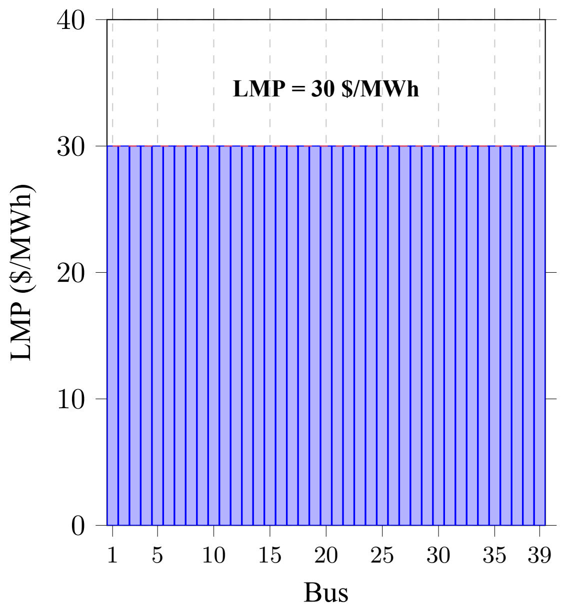

Figure 6: Locational marginal prices (LMPs) for the IEEE 39-bus system under uncongested conditions.
Source: created by the authors

The Figure 7 summarizes the results of the DC-OPF solution for the IEEE 39-node system with an optimal objective value of $z = 1704.55$. Under these conditions, the LMPs are uniform across all nodes, with a value of 30.00 $/MWh$, since no transmission limits are active and all line shadow prices μ are zero. The generation is mainly supplied by four units, with Node 39 providing 4650.5 MW, Node 31 and Node 37 each generating 595 MW, and Node 34 producing 255 MW, while the remaining units are not dispatched. Selected line flows are also reported in per unit, indicating balanced power distribution without congestion. These results provide the base case for subsequent analysis of nodal prices under transmission constraints.

The congested DC-OPF yields an optimal objec-

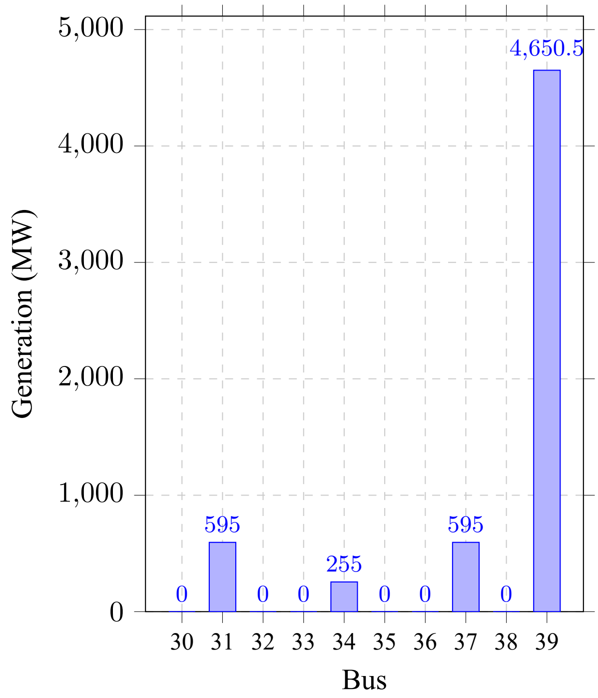

Figure 7: Generator dispatch results obtained from the DC-OPF model.
Source: created by the authors

tive value of z=1879.30, reflecting the additional operational cost induced by active transmission bottlenecks. The resulting nodal prices exhibit a markedly non-uniform pattern, with LMPs spanning from 20 to 40$/MWh, evidencing the presence of binding constraints and spatial marginal cost differentiation. In the Figure 8 lowest prices arise at Nodes 31 and 37 (20 $/MWh), indicating electrically favorable locations with unconstrained access to low-cost generation. Intermediate values of 35 $/MWh appear at Nodes 1, 9, 32, and 36, suggesting moderate proximity to congestion interfaces. In contrast, most of the network settles at the upper bound of 40 $/MWh, including Nodes 2–8, 10–21, 24–30, 33–34, and 38, where congestion forces the system to dispatch costlier marginal resources. Two nodes (22 and 23) present marginally lower prices (39.9998 $/MWh), consistent with numerically binding flow limits. Finally, Node 35 exhibits a distinct intermediate price of 37 $/MWh, while Node 39, typically the main supply point of the 39-bus system, clears at 30 $/MWh. Overall, the LMP dispersion sharply contrasts with the uniform-price case, confirming that transmission congestion creates pronounced spatial price signals aligned with the physical constraints of the grid.

In the Fgure 9 illustrates the optimal generation schedule under congestion reveals a highly differentiated dispatch pattern driven by marginal costs

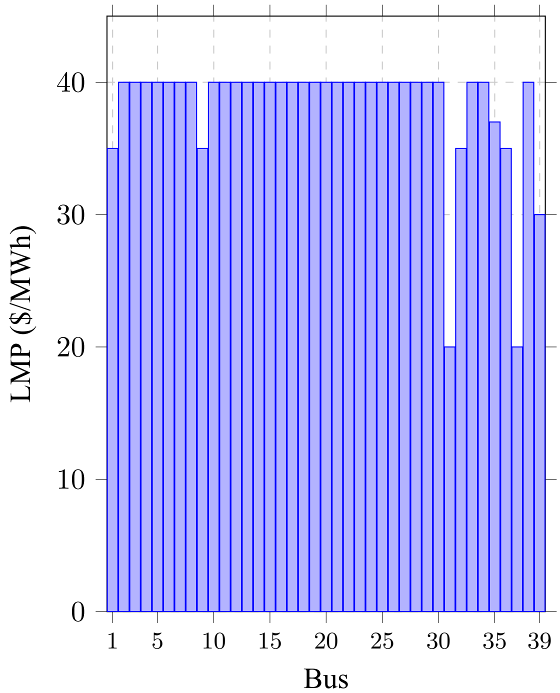

Figure 8: Locational marginal prices (LMPs) for the IEEE 39-bus system.
Source: created by the authors

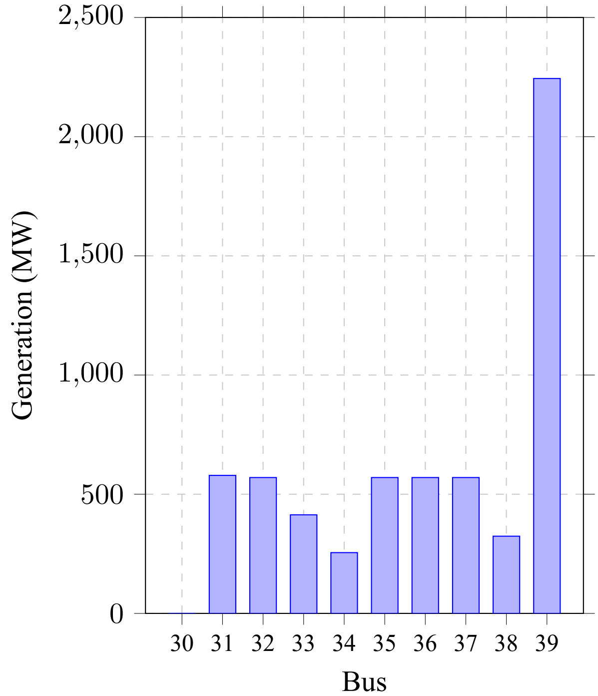

Figure 9: Generator dispatch results obtained from the DC-OPF model under Scenario 2.
Source: created by the authors

and transmission limitations. The largest contribution originates from Bus 39, delivering 2244 MW, which aligns with its role as a major low-cost supplier in the IEEE 39-bus benchmark. A second cluster of generators—located at Buses 31, 32, 35, 36, and 37—operates close to their nominal upper limits, each producing approximately 570 MW, indicating that these units become economically attractive once congestion shifts the marginal price across the network. Additional mid-range contributions are observed at Bus 33 (414 MW) and Bus 38 (324 MW), which help balance the system near congested corridors. In contrast, Bus 34 provides a modest 255 MW, suggesting that local conditions or marginal cost differentials restrict its full utilization. Finally, Bus 30 contributes virtually zero output (0.001 MW), confirming that this unit is priced out of the market under the prevailing LMP structure. Overall, the dispatch profile reflects the coordinated interplay between generator cost parameters and network congestion, leading to a spatially efficient yet highly uneven utilization of available resources.

Figure 10 reports the shadow prices associated with transmission capacity limits. Only a small subset of lines exhibits binding conditions. In particular, lines (06–31) and (25–37) present high congestion values (20 $/MWh), indicating strong marginal value for additional capacity. Lines (01–02), (01–39), (08–09), (09–39), (10–32), and (23–36) show moderate congestion (5 $/MWh). All other lines remain non-binding.

Figure 11 presents the results of DC Model 2 considering transmission congestion and network losses. The DC-OPF results for this operating scenario yield an optimal objective value of z = 1906.34, slightly lower than the previous configuration, yet still indicative of substantial congestion across the network. The resulting LMP profile displays a pronounced spatial gradient, with prices ranging from 20.0 to 52.48 $/MWh, underscoring the presence of binding transmission constraints and the emergence of distinct marginal cost zones throughout the IEEE 39-bus system.

The minimum prices arise at Nodes 31 (20.00 $/MWh) and 37 (20.91 $/MWh), reflecting isolated regions with access to inexpensive supply and minimal interaction with congested interfaces. Slightly higher values appear at Nodes 32 (35.26 $/MWh) and 36 (35.68 $/MWh), along with Node 35 (37.57 $/MWh), forming an intermediate cost region where nodes remain partially shielded from congestion effects.

A broad plateau between 41 and 43 $/MWh encompasses Nodes 16–24, 26–30, and several nodes in the central corridor. This cluster represents the network's structural backbone, where congestion re-

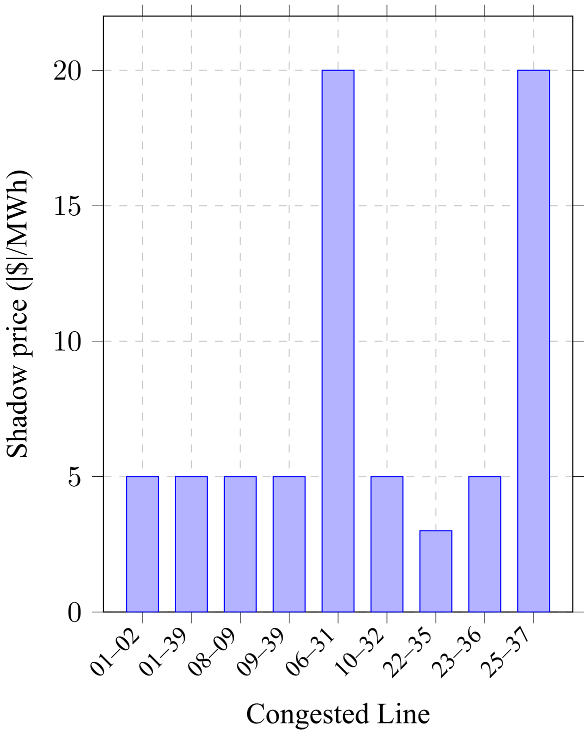

Figure 10: Binding transmission capacity constraints: absolute value of shadow prices (DC-OPF).
Source: created by the authors

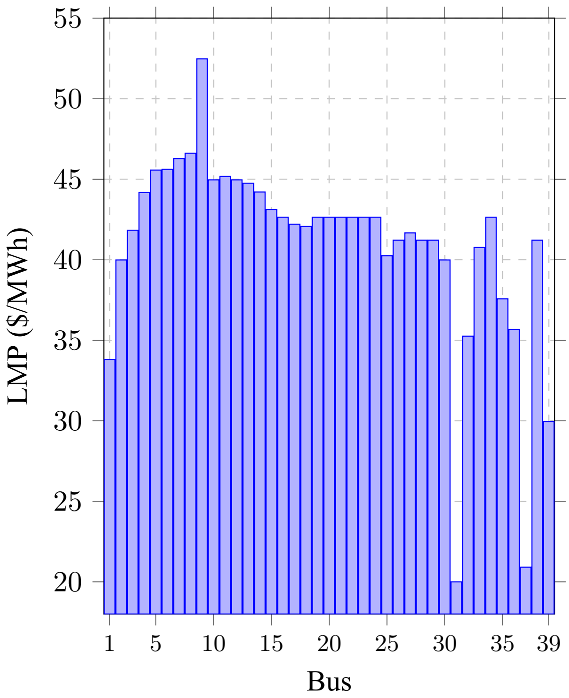

Figure 11: Locational marginal prices (LMPs) for the IEEE 39-bus system under Scenario 4.
Source: created by the authors

distributes marginal energy costs in a relatively consistent manner. Additional mid-range prices appear at Node 25 (40.25 $/MWh) and Node 33 (40.76 $/MWh), indicating local variations tied to flow patterns and topological proximity to bottlenecks.

Higher LMP values concentrate in the northeastern area, particularly at Nodes 3–15, where prices escalate from 41.83 $/MWh (Bus 3) up to 46.61 $/MWh (Bus 8). These nodes bear the brunt of congestion-driven redispatch, with the price peak observed at Node 9, reaching 52.48 $/MWh, making it the system's most constrained location under this scenario.

Finally, Node 39—typically a major low-cost generation source—settles at 29.96 $/MWh, consistent with its role in anchoring the lower bound of the marginal cost structure.

Overall, the LMP distribution reveals a system under significant congestion stress, characterized by steep marginal cost differentials and clear segmentation into low-, medium-, and high-price regions. The price spike at Node 9 once again highlights its position as a critical bottleneck, shaping the economic and operational outcomes of the dispatch.

In the Figure 12 illustrates the optimal dispatch results exhibit a distinct allocation of generation across the network, reflecting the influence of marginal production costs and active congestion constraints. The dominant supplier in the system remains Bus 39, producing 1864.8 MW, consistent with its role as a large and economically efficient generating unit. A second tier of high-output generators—including Buses 32, 33, 35, 36, and 37—operates at or near their maximum available capacity, each contributing 570 MW. This behavior indicates that these units become marginally competitive once congestion reshapes the system's marginal cost structure.

Intermediate levels of production appear at Bus 38, supplying 546.7 MW, and Bus 31, generating 524.6 MW. These units serve as transitional resources, filling the gap between the heavily utilized low-cost generators and the more constrained nodes. Meanwhile, Bus 34 contributes a modest 255 MW, likely reflecting a combination of local marginal cost and limited downstream demand relief under network constraints.

Finally, Bus 30 remains fully out of the economic dispatch, producing effectively 0 MW, which is consistent with being priced out of the market under the prevailing LMP conditions.

Overall, the generation pattern reveals a system strongly shaped by network congestion, with heavy reliance on a core group of low-cost units while mid-range generators absorb redispatch effects. The resulting dispatch structure highlights the interplay between spatial marginal costs and transmission limitations in the IEEE 39-bus system.

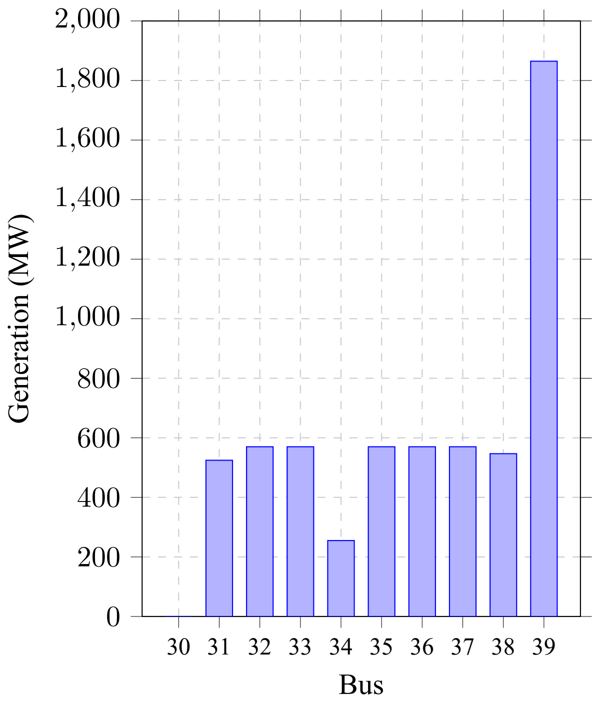

Figure 12: Generator dispatch results obtained from the DC-OPF model under Scenario 5.
Source: created by the authors

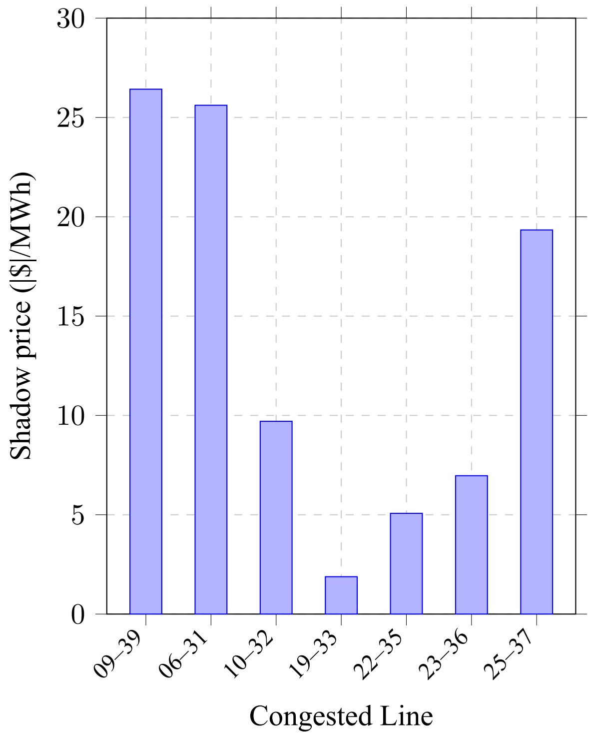

Figure 13: Binding transmission constraints: absolute shadow prices for Scenario 6 (DC-OPF).
Source: created by the authors

In the Figure 13 illustrates the analysis of the transmission-line shadow prices shows that virtually all corridors operate strictly within their thermal limits, with μ^+ and μ^- values equal to zero across most branches, indicating non-binding constraints with no impact on nodal marginal prices. Congestion emerges only on a small set of critical interfaces, where non-zero μ^- values reveal binding directional limits that actively shape the LMP structure: the strongest bottlenecks occur on Bus 09→Bus 39 ($\mu^- = -26.42$) and Bus 06→31 ($\mu^- = -25.61$), followed by Bus 25→Bus 37 ($\mu^- = -19.34$), Bus 10→Bus 32 ($\mu^- = -9.70$), Bus 23→Bus 36 ($\mu^- = -6.96$), Bus 22→Bus 35 ($\mu^- = -5.07$), and Bus 19→Bus 33 ($\mu^- = -1.88$). These shadow prices quantify the marginal benefit of relaxing each line limit, highlighting that reinforcing the most constrained corridors—particularly 09–39 and 06–31—would produce the largest reductions in system operating cost and significantly reduce LMP dispersion. Overall, the dual patterns confirm that the observed price differentials originate from a few strategically congested pathways that govern the spatial distribution of marginal costs in the IEEE 39-bus system.

4 Discussion of Results

The kernel density estimates in Fig. 14 highlight the progressive dispersion of nodal prices as physical constraints are introduced. In the base case, the density collapses into a spike at 30 $/MWh, reflecting a single-bus market. When line capacity limits are enforced, the distribution widens and becomes slightly bimodal, with a dominant mass around 40 $/MWh and a secondary concentration close to 20–35 $/MWh. Under simultaneous congestion and losses, the density further spreads towards higher values and develops a heavier right tail, with a non-negligible probability of prices above 50 $/MWh, which is consistent with the increased marginal cost of delivering power to stressed areas of the network.

The results obtained from the DC-OPF without congestion indicate that all nodal prices remain perfectly uniform at 30 $/MWh, as no transmission limits are binding and line losses are neglected. In this configuration, the dispatch relies entirely on the cheapest available generating units, and every bus faces the same marginal energy cost. This scenario serves as the economic baseline for evaluating how physical constraints modify system behavior under more realistic operating conditions.

When transmission capacities are enforced, the uniform pricing pattern disappears even though losses are still neglected. Under this scenario, nodal prices span a wider range, from 20 $/MWh (buses 31 and 37) up to 40 $/MWh, which becomes the dominant

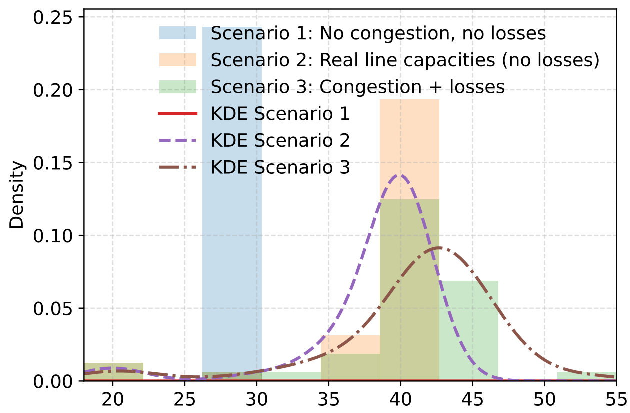

Figure 14: Density LMPs
Source: created by the authors

marginal price across most nodes. Intermediate values such as 35 \$/MWh and 37 \$/MWh appear at several buses, reflecting localized system stress. This dispersion results solely from transmission bottlenecks, demonstrating how congestion alters marginal energy costs and forces redispatch across the network even in the absence of losses.

When both congestion and losses are incorporated, the price dispersion increases significantly. Nodal prices range from 20.00 \$/MWh (node 31) to 52.48 \$/MWh (node 9), representing the widest spread among all scenarios. Several nodes cluster around 42.64 \$/MWh, while others experience higher marginal costs driven by loss factors and binding constraints. In this operating condition, congestion in multiple corridors and the presence of marginal losses simultaneously shape LMP formation. The resulting economic signals reflect not only energy reallocation due to transmission congestion but also the incremental cost of delivering power to distant or heavily loaded areas. This confirms the importance of jointly modeling congestion and losses to represent system conditions accurately and derive meaningful market outcomes.

5 Scientific Contribution

This study contributes to the state of the art in nodal pricing by proposing a hybrid AC–DC workflow that embeds physically accurate loss modeling into a computationally efficient DC-OPF formulation. First, AC power-flow simulations in DIgSILENT PowerFactory are used to derive systemwide losses and construct marginal generation and demand loss factors (LF_g, LF_d) based on distribution factors obtained from the incidence matrix A and the susceptance matrix Y. These AC-consistent loss factors are then integrated into the DC-OPF constraints, together with a calibrated *OFFSET* term that guarantees exact closure of the global power-balance equation and eliminates the systematic bias typically observed in loss-adjusted DC models.

Unlike conventional DC-OPF approaches—which either ignore losses or apply simplified ex-post corrections—our formulation incorporates marginal losses *within* the market-clearing optimization. This ensures transparent, economically meaningful locational marginal price (LMP) signals while preserving the tractability of DC methods. The proposed workflow is fully reproducible, bridging commercial simulation tools (DIgSILENT) with open-source optimization (Pyomo), and enabling researchers, regulators, and system operators to evaluate nodal prices under realistic network conditions.

Validation on a three-bus system and the IEEE 39-bus benchmark demonstrates that the method accurately captures the joint impact of congestion and marginal losses, producing LMP dispersion patterns consistent with physical constraints and economic theory. Shadow-price analysis confirms the interpretability of dual variables, while density-based comparisons across scenarios highlight the progressive widening of price differentials as constraints become active. Overall, the methodology provides a scalable, auditable, and physically grounded framework for modern electricity-market studies.

6 Conclusion

The baseline DC-OPF case (no active limits and no losses) yields perfectly uniform LMPs of 30 \$/MWh across all buses, with a dispatch configuration driven by the lowest cost units. This confirms marginal cost consistency when the network operates without congestion: prices exhibit no locational differentiation, and the resulting power transfers remain feasible without thermal stress. The outcome provides a reproducible reference point for evaluating the effects of transmission constraints and losses. It also validates the DIgSILENT $\rightarrow$ Pyomo data pipeline, ensuring that subsequent price variations can be attributed to physical constraints rather than numerical artifacts. In short, this scenario acts as a clean and controlled baseline before introducing real-world frictions.

Enforcing real transmission capacities breaks this uniformity even in the absence of losses. Under this scenario, LMPs span from 20 \$/MWh (e.g., nodes 31 and 37) to 40 \$/MWh, which dominates most buses due to congestion-induced redistribution of marginal costs. The dispatch shifts toward additional units notably those located at nodes 32-38 reflecting the cost of relieving constrained corridors. Higher prices arise downstream of bottlenecks where network capacity is scarce, while lower prices remain in areas with unconstrained access to low-cost generation.

These results reinforce the economic interpretation of dual variables as shadow prices of transmission limits, highlighting the importance of network-aware pricing even within a simplified DC formulation.

When both congestion and losses are considered, LMP dispersion increases substantially. Prices range from 20.00 \$/MWh (slack bus) to 52.48 \$/MWh (node 9), the largest spread among all scenarios. Incorporating generation and demand loss factors (LF_g, LF_d) derived from

$$H = YA\left(A^{\top}YA\right)^{-1}$$

together with an OFFSET calibration term aligns the DC formulation with AC-estimated losses, preventing systematic bias in LMPs. Marginal losses reorder the relative merit of generators located at nodes 32-39, while congestion in multiple corridors amplifies locational differentials. The workflow is auditable and reproducible, generating physically grounded and economically meaningful signals for planning studies, tariff design, and welfare analysis. Overall, losses matter in two dimensions: economically, through their impact on prices; and physically, through their influence on dispatch.

Adopting the AC$\rightarrow$DC workflow with LF_g/LF_d and an OFFSET calibration term is recommended as a practical standard for market and operational studies: it balances physical traceability with computational tractability. Future extensions may include joint optimization of energy and ancillary services, incorporation of ramping and unit-commitment constraints, and stochastic or robust formulations to capture uncertainty from renewables, demand variability, and outages. Validation with real SCADA/EMS data and AC-OPF benchmarks would further strengthen regulatory acceptance and operational credibility. For system operators and regulators, the approach provides clearer, reliability aligned LMP signals; for researchers, it offers a transparent bridge between detailed AC physics and scalable market-clearing models.

References:

[1] Z. Y. Dong and Y. Zhang, "Interdisciplinary vision of the digitalized future energy systems," *IEEE Open Access Journal of Power and Energy*, vol. 8, pp. 557–569, 2021, https://doi.org/10.1109/OAJPE.2021.3108937.

[2] R. Weron, "Electricity price forecasting: A review of the state-of-the-art with a look into the future," *International Journal of Forecasting*, vol. 30, no. 4, pp. 1030–1081, 2014, https://doi.org/10.1016/j.ijforecast.2014.08.008.

[3] B. Stott, J. Jardim, and O. Alsac, "Dc power flow revisited," *IEEE Transactions on Power Systems*, vol. 24, no. 3, pp. 1290–1300, 2009, https://doi.org/10.1109/TPWRS.2009.2021235.

[4] H. Liu, L. Tesfatsion, and A. A. Chowdhury, "Locational marginal pricing basics for restructured wholesale power markets," in *2009 IEEE Power & Energy Society General Meeting*, 2009, pp. 1–8, https://doi.org/10.1109/PES.2009.5275503.

[5] M. Ndrio, A. Winnicki, and S. Bose, "Pricing economic dispatch with ac power flow via local multipliers and conic relaxation," *IEEE Transactions on Control of Network Systems*, vol. 11, no. 3, pp. 1704–1716, 2024, https://doi.org/10.1109/TCNS.2022.3203470.

[6] Z. Yuan, M. R. Hesamzadeh, and D. R. Biggar, "Distribution locational marginal pricing by convexified acopf and hierarchical dispatch," *IEEE Transactions on Smart Grid*, vol. 9, no. 4, pp. 3133–3142, 2018, https://doi.org/10.1109/TSG.2016.2627139.

[7] D. P. Brown, D. E. Olmstead, and B. Shaffer, "Electricity market design with increasing renewable generation: Lessons from alberta," *The Electricity Journal*, p. 107484, 2025, https://doi.org/10.1016/j.tej.2025.107484.

[8] S. Biswas, B. Çavdar, A. Garcia, and J. Geunes, "The price of flexibility in electricity markets," *Energy Economics*, vol. 150, p. 108769, 2025, https://doi.org/10.1016/j.eneco.2025.108769.

[9] X. Ai, J. Wu, J. Hu, Z. Yang, and G. Yang, "Distributed congestion management of distribution networks to integrate prosumers energy operation," *IET Generation, Transmission & Distribution*, vol. 14, no. 15, pp. 2988–2996, 2020, https://doi.org/10.1049/iet-gtd.2019.1110.

[10] L. Bai, J. Wang, C. Wang, C. Chen, and F. Li, "Distribution locational marginal pricing (dlmp) for congestion management and voltage support," *IEEE Transactions on Power Systems*, vol. 33, no. 4, pp. 4061–4073, 2018, https://doi.org/10.1109/TPWRS.2017.2767632.

[11] E. Litvinov, T. Zheng, G. Rosenwald, and P. Shamsollahi, "Marginal loss modeling in lmp calculation," *IEEE Transactions on Power Systems*, vol. 19, no. 2, pp. 880–888, 2004, https://doi.org/10.1109/TPWRS.2004.825894.

[12] K. Verma and H. Gupta, "Impact on real and reactive power pricing in open power

market using unified power flow controller," *IEEE Transactions on Power Systems*, vol. 21, no. 1, pp. 365–371, 2006, https://doi.org/10.1109/TPWRS.2005.857829.

[13] T. Gedra, "On transmission congestion and pricing," *IEEE Transactions on Power Systems*, vol. 14, no. 1, pp. 241–248, 1999, https://doi.org/10.1109/59.744539.

[14] U. Liyanapathirane, M. Khorasany, and R. Razzaghi, "Optimization of economic efficiency in distribution grids using distribution locational marginal pricing," *IEEE Access*, vol. 9, pp. 60 123–60 135, 2021, https://doi.org/10.1109/ACCESS.2021.3073641.

[15] Z. Zhao, Y. Liu, L. Guo, L. Bai, Z. Wang, and C. Wang, "Distribution locational marginal pricing under uncertainty considering coordination of distribution and wholesale markets," *IEEE Transactions on Smart Grid*, vol. 14, no. 2, pp. 1590–1606, 2023, https://doi.org/10.1109/TSG.2022.3200704.

[16] Z. Zhao, Y. Liu, L. Guo, L. Bai, and C. Wang, "Locational marginal pricing mechanism for uncertainty management based on improved multi-ellipsoidal uncertainty set," *Journal of Modern Power Systems and Clean Energy*, vol. 9, no. 4, pp. 734–750, 2021, https://doi.org/10.35833/MPCE.2020.000824.

[17] W. Zhong, K. Xie, Y. Liu, S. Xie, and L. Xie, "Nash mechanisms for market design based on distribution locational marginal prices," *IEEE Transactions on Power Systems*, vol. 37, no. 6, pp. 4297–4309, 2022, https://doi.org/10.1109/TPWRS.2022.3152517.

[18] P. Andrianesis, D. Bertsimas, M. C. Caramanis, and W. W. Hogan, "Computation of convex hull prices in electricity markets with non-convexities using dantzig-wolfe decomposition," *IEEE Transactions on Power Systems*, vol. 37, no. 4, pp. 2578–2589, 2022, https://doi.org/10.1109/TPWRS.2021.3122000.

[19] A. Winnicki, M. Ndrio, and S. Bose, "On convex relaxation-based distribution locational marginal prices," in *2020 IEEE Power and Energy Society Innovative Smart Grid Technologies Conference (ISGT)*, 2020, pp. 1–5, https://doi.org/10.1109/ISGT45199.2020.9087752.

[20] C. Quinatoa, I. Valencia, A. Casilimas, and A. Garcés, "A convex optimization model for bidirectional vehicle-to-grid operation," in *2018 IEEE ANDESCON*, 2018, pp. 1–7, https://doi.org/10.1109/ANDESCON.2018.8564695.

[21] J. S. Ortiz, C. I. Quinatoa, and J. H. Acurio, "A new model optimization convex using wirtinger calculus for economic dispatch," in *2024 8th International Conference on Power Energy Systems and Applications (ICoPESA)*, 2024, pp. 557–566, https://doi.org/10.1109/ICOPESA61191.2024.10743906.

[22] L. Tesfatsion, "Locational marginal pricing: A fundamental reconsideration," *IEEE Open Access Journal of Power and Energy*, vol. 11, pp. 104–116, 2024, https://doi.org/10.1109/OAJPE.2024.3361751.

[23] M. J. Mustapha and G. Taylor, "Investigation and evaluation of the adoption of locational marginal pricing in electricity markets," in *2023 58th International Universities Power Engineering Conference (UPEC)*, 2023, pp. 1–6, https://doi.org/10.1109/UPEC57427.2023.10294709.

[24] H. Ming, A. A. Thatte, and L. Xie, "Revenue inadequacy with demand response providers: A critical appraisal," *IEEE Transactions on Smart Grid*, vol. 10, no. 3, pp. 3282–3291, 2019, https://doi.org/10.1109/TSG.2018.2822778.

[25] M. Kaleta, "A generalized class of locational pricing mechanisms for the electricity markets," *Energy Economics*, vol. 86, p. 103455, 2020, https://doi.org/10.1016/j.eneco.2016.09.023.

[26] Z. Tan, T. Cheng, Y. Liu, and H. Zhong, "Extensions of the locational marginal price theory in evolving power systems: A review," *IET Generation, Transmission & Distribution*, vol. 16, no. 7, pp. 1277–1291, 2022, https://doi.org/10.1049/gtd2.12381.

[27] A. Venzke, S. Chatzivasileiadis, and D. K. Molzahn, "Inexact convex relaxations for ac optimal power flow: Towards ac feasibility," *Electric Power Systems Research*, vol. 187, p. 106480, 2020, https://doi.org/10.1016/j.epsr.2020.106480.

[28] X. Bai, L. Qu, and W. Qiao, "Robust ac optimal power flow for power networks with wind power generation," *IEEE Transactions on Power Systems*, vol. 31, no. 5, pp. 4163–4164, 2016, https://doi.org/10.1109/TPWRS.2015.2493778.

[29] A. Peña-Ordieres, D. K. Molzahn, L. A. Roald, and A. Wächter, "Dc optimal power flow

with joint chance constraints," *IEEE Transactions on Power Systems*, vol. 36, no. 1, pp. 147–158, 2021, https://doi.org/10.1109/TPWRS.2020.3004023.

[30] DIgSILENT GmbH, *DIgSILENT PowerFactory 2021 User Manual*, DIgSILENT GmbH, Gomaringen, Germany, 2021, https://www.digsilent.de/en/downloads.html.

[31] W. E. Hart, C. D. Laird, J.-P. Watson, D. L. Woodruff, G. A. Hackebeil, B. L. Nicholson, and J. D. Siirola, *Pyomo Optimization Modeling in Python*, ser. Springer Optimization and Its Applications. Springer, 2017, vol. 67, https://doi.org/10.1007/978-3-319-58821-6.

[32] J. Yang, Z. Y. Dong, and F. Wen, "A comparative study of marginal loss pricing algorithms in electricity markets," *IET Generation, Transmission & Distribution*, vol. 15, no. 3, pp. 576–588, 2021, https://doi.org/10.1049/gtd2.12030.

[33] D. Kirschen and G. Strbac, *Fundamentals of Power System Economics*. Hoboken, NJ, USA: Wiley, 2014.

[34] C. Quinatoa, A. Chasi, V. Puetate, A. Casilimas, L. Camacho, and J. Ortiz, "Optimization model for coordinated multistage planning of the generation-transmission system with demand forecasting using neural networks," in *Proceedings of the 4th International Conference on Electronic Engineering and Renewable Energy Systems—Volume 1*, B. Hajji, A. Gagliano, A. Mellit, A. Rabhi, and M. Calì, Eds. Singapore: Springer Nature Singapore, 2025, pp. 573–581.

[35] P. Kundur, *Power System Stability and Control*. New York: McGraw-Hill, 1994, the IEEE 39-bus New England test system is described and used in several chapters.

Contribution of Individual Authors to the Creation of a Scientific Article (Ghostwriting Policy)

The authors equally contributed in the present research, at all stages from the formulation of the problem to the final findings and solution.

Sources of Funding for Research Presented in a Scientific Article or Scientific Article Itself

No funding was received for conducting this study.

Conflict of Interest

The authors have no conflicts of interest to declare that are relevant to the content of this article.